Chapter 5

Applications

Summary

Chapter 5 gives a flavor of possible applications of the extended O'Doherty-Anstey theory to 2-D and 3-D random media. Generally, the here presented theory has the same range of application than the generalized O'Doherty-Anstey theory of 1-D random media. Provided that a statistical macro model is available that includes information of small-scale heterogeneities and therefore complement the macro models of large-scale structures like seismic 'reflectors', then the ODA theory allows to quantify the effects of these heterogeneities on the primary wave field. Statistical information of small-scale heterogeneities can be extracted from well-logs or statistical wave field analysis. Together with such statistical macro models the extended ODA theory improves migration and inversion results.

In section (5.1) we show how reliable estimates of scattering attenuation in complex geological regions are obtained with help of statistical information from borehole data. The scattering attenuation model of section (3.6) is applied to the German KTB region. In particular, we show that the measured low Q-values inferred from P-waves of the VSP experiment can be explained to a considerable amount as scattering attenuation (see also Müller and Shapiro, 2001b). This is contradictory to previous studies that explain the measured attenuation in terms of absorption mechanisms.

Section (5.2) presents first results of the application of the Green's function in order to correct for transmission losses due to complex overburden of reflectors. The correction is incorporated in the true-amplitude migration technique and in an idealized AVO study of synthetic data, referring to a model of the subducting Nazca plate in South America. With help of the proposed correction method, constraints of the magnitudes of reflection coefficients can be found. A part of the results is submitted for publication (see Buske et al., 2001, and Sick et al., 2001).

5.1 Interpretation of scattering attenuation in the KTB area

Fundamental signatures of seismic waves in rocks are the attenuation and the dispersion. It is of great importance for the interpretation of seismic data to quantify the magnitude as well as the frequency dependence of attenuation. The knowledge of attenuation is needed for a correct estimation of the magnitude of reflection coefficients. From a practical point of view, there are however serious problems connected with the determination of attenuation (Bourbié et al., 1987). One of them is the fact that, in general, attenuation is not only caused by absorption, i.e. due to viscoelastic effects (anelasticity, presence of fluids) but also due to the heterogenous composition of rocks and reservoirs on many length scales. A further difficulty is the frequency dependence of attenuation measurements. That is why laboratory experiments cannot easily be compared with field measurements.

It is well-known that inhomogeneities of any scale affect the seismic wave field and characteristics of scattering attenuation and dispersion are observed like e.g. the decrease of seismogram amplitudes with increasing travel-distance and the broadening of seismic pulses. In contrast to attenuation by absorption (sometimes called intrinsic attenuation), where the energy of the wave field is transferred into heat, scattering attenuation means a spatial redistribution of wave field energy. So that at a certain recording position only a part of the wave field energy can be received within a certain time interval. The signals seem apparently damped (apparent attenuation).

Usually the attenuation of seismic wave fields are characterized with help of the quality factor Q (see Bourbié et al., 1987, for a detailed exposition of the quality factor concept). In general, Q-values inferred from seismic data sets include both kinds of attenuation. In many studies it is assumed that the total reciprocal quality factor can be obtained by superposition of the reciprocal quality factors related to a certain attenuation mechanism. There are also some efforts to separate the intrinsic part from the scattering attenuation part. This is, however, not an easy task, especially in reservoir geophysics, because a priori it is not known which absorption mechanisms are present nor how the geometrical composition of rocks looks like.

It is the purpose of this study to apply the new model of scattering attenuation (section 3.6) to the KTB area, where statistical estimates from the boreholes are used in order to quantify the amount of scattering attenuation. In contrast to previous studies, where the scattering attenuation estimate of based on the traveltime-corrected mean field formalism (Sato and Fehler, 1998) was found to be insignificant (e.g. Holliger, 1997), we show that the measured Q-values can be explained to a considerable amount due to scattering on uppercrustal heterogeneities.

5.1.1 Attenuation measurements at the KTB-site

Within the framework of the KTB (the German continental deep drilling project) a new insight in the structure of the continental crust was obtained. The KTB-site is located in Southeastern Germany and consists of two super-deep boreholes. The rocks are of crystalline type (for a thorough review of this project we refer to Harjes et al., 1997). Several techniques (including analysis of VSP-Data and lab measurements) have been applied in order to estimate the attenuation of P- and S-waves (see also Pujol et al., 1998 for a review). Figure

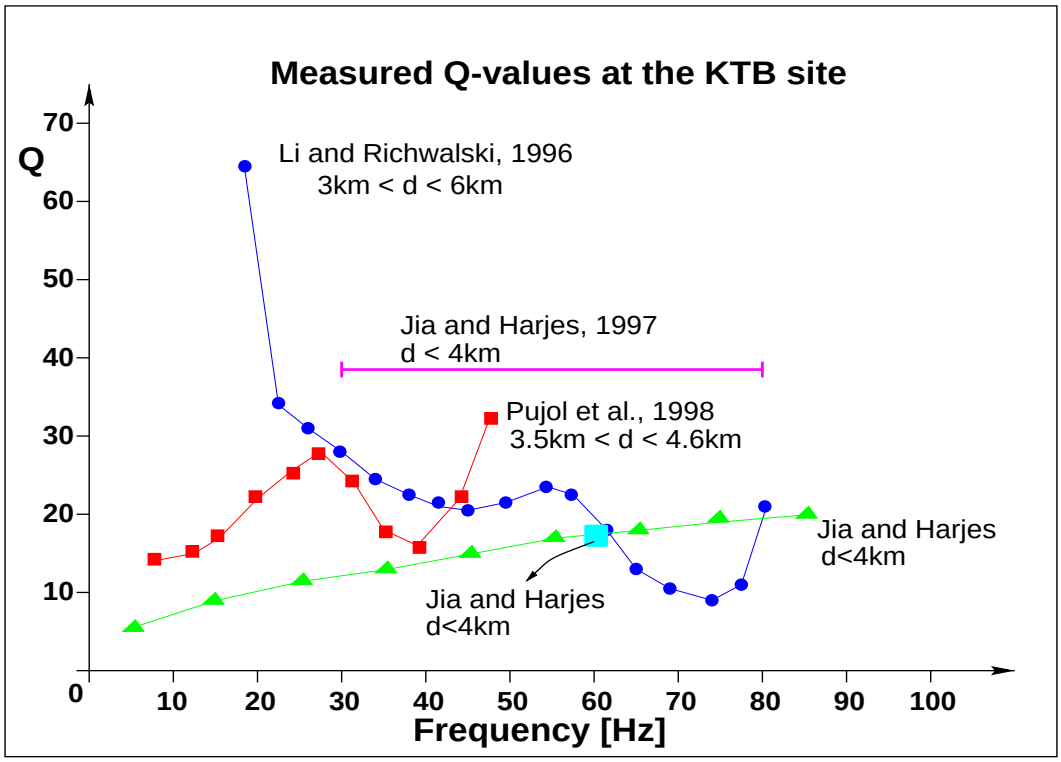

Figure 5.1: Measured Q-values of P-waves at the KTB-site and the corresponding reference. The depth range is denoted by d.

(5.1) displays the measured Q-values resulting from P-waves attenuation in the frequency range from 5 to 85 Hz and indicates the corresponding references and depth intervals d. In summary, all studies show surprisingly low Q-values ($Q < 100$). Note that reported Q-values of the lithosphere are of the order $Q = 100 - 1000$ (see e.g. Figure 5.2 in Sato and Fehler, 1998).

In order to interpret these low Q-values several attenuation mechanisms have been assumed to play a major role at the KTB-site. Lüschen et al. (1996) argued that lithology contrasts do not cause strong reflections (so that scattering attenuation is small). Strong reflections are related to fluid-filled fracture systems. Pujol et al. (1998) argued that scattering due to thin layering is not a dominant effect of attenuation. Holliger (1997) used the 2-D single scattering model together with seismic velocity fluctuation statistics based on well-logs in order to estimate uppercrustal scattering Q-values ranging between 600 and 1500. He concluded that the attenuation is dominated by absorption rather than by scattering.

5.1.2 Application of the new scattering attenuation model

We study whether the relatively low Q-values can be explained due to scattering. That is to say, we apply the scattering attenuation model as derived in section (3.6) to the KTB-site. Fortunately, a statistical analysis of the well-logs (Vp, Vs and density) and VSP data yielding estimates of characteristic sizes of heterogeneities (correlation lengths a) and contrasts (relative standard deviations σ_r of the background P-wave velocity c_0) have been already performed. The results are briefly summarized in the following table:

Statistical parameter estimates from log-data at the KTB-site			
reference	depth range ($[z] = m$)	type of correlation function	parameters ($[c_0] = km/s, [a] = m$)
Wu et al., 1994	286-6000	von Kármán (2-D), anisotropic $\frac{a_x}{a_z} \approx 1.8$	$\nu_z = 0.05$, $\nu_x = 0.5$ $a_z = 2000$, $a_x = 3600$ $\sigma = 6.1 - 6.5\%$, $P : c_0 = 6.1$
Kneib, 1995	285-6000	superposition of 2 exponential, isotropic	$a_1 = 1$, $a_2 = 20$ $\sigma = 2.9 - 3.4\%$ $P : c_0 = 6.4$, S: $c_0 = 3.53$
Holliger, 1996, 1997, Jones & Holliger, 1997	285-7200	von Kármán (3-D) isotropic $\frac{a_x}{a_z} \approx 1$	$\nu = 0.1 - 0.2$ $a = 60 - 160$ $\sigma = 3.2 - 6.3\%$, $P : c_0 = 6.3$

Moreover, Jones and Holliger (1997) investigate the inter-log coherence and find no significant correlation between the sonic logs from the pilot and main hole, which are located 200 m apart. They conclude that the lateral correlation length is smaller than 200 m and is approximately the same as the vertical correlation length. These studies justify the assumption that the upper crust heterogeneities can be well characterized as a realization of an isotropic random medium using spatial correlation functions. This assumption has been made not only for the KTB-site but also for many regions. Especially the fractal-like character of upper crustal heterogeneities may be accommodated by the use of a von Kármán correlation function (see Sato and Fehler, 1998). Goff and Holliger (1999) showed that the superposition of four von Kármán processes yields an even better characterization of the velocity fluctuations. Restricting to a single-scale random medium, we choose a von Kármán correlation function which is additionally characterized by the so-called Hurst number ν. Its fluctuation spectrum in 3-D is given by

$$\Phi^{3D}(\kappa) = \frac{\sigma^2\, a^3\, \Gamma(\nu + 1.5)}{\pi^{1.5}\, \Gamma(\nu)\, (1 + \kappa^2 a^2)^{\nu+1.5}}\,. \tag{5.1}$$

For $\nu = 1/2$ one obtains an exponential correlation function. Note that equation (5.1) differs from somewhere used definitions of the fluctuation spectrum (factor $8\pi^3$ due to different definition of the spatial Fourier transform).

As the Q-measurements result from VSP-data we must further make sure that the weak wave field scattering regime, where our scattering model is valid, is a reasonable assumption. The scattering regime is characterized by 3 parameters, namely the dimensionless wavenumber ka, the normalized travel-distance L/a and the strength of the velocity perturbations (i.e., the relative standard deviation σ). Kneib (1995) shows that the relevant frequencies in the VSP experiment ($f = 30Hz$) and the inferred correlation length lead to $ka > 0.6$. Taking into account the geometry of the experiment one obtains $L/a = 15 - 400$. Together with the estimated relative standard deviations ($\sigma_r < 7\%$), we conclude that the weak scattering assumption is fully justified. The regime, where the wave field fluctuations become saturated, is not realizable within the given VSP experiment. This becomes intuitively clear when looking at the VSP seismograms like in Figure 17 of Kneib (1995), where the wave field amplitudes after the first arrivals are small and the wavefront is not strongly distorted.

Next we compute the quality factor as a function of frequency for waves excited by a point source in 3-D using formula (3.50) together with equation (5.1) and noting that $Q = k/(2\alpha)$. The impact of the parameters Hurst number, standard deviation, correlation length and travel-distance are studied (Fig. (5.2)). The parameters are chosen according to the inferred values from the well log analysis. First we let vary the Hurst number from $\nu = 0.1 - 0.5$ for fixed values of $L = 7km$, $c_0 = 6350m/s$, $\sigma_r = 5.5\%$ and $a = 160m$ (upper left-sided plot in Fig. (5.2)). An increased scattering attenuation can be observed for increasing Hurst coefficients. If $\nu = 0.5$ the complete measured attenuation could be explained due to scattering attenuation. This value of ν, however, is according to the statistical estimates too high. Then we study the influence of the relative standard deviation of the velocity fluctuations (upper right-sided plot in Fig. (5.2)), where we use the same fixed values as above and choose $\nu = 0.2$. The relative standard deviation of the velocity fluctuations shows a strong influence on the magnitude of attenuation. For large standard deviations ($\sigma_r > 7\%$) we observe again that the complete measured attenuation is due to scattering (this is of course an unrealistic situation and defines an upper bound of σ_r). We are further interested in the dependency on the correlation length (lower left-sided plot in Fig. (5.2)). As the estimates from the KTB boreholes suggest, we consider realistic values of a ranging from 60 to $250m$. Finally the lower plot on the right side of Fig. (5.2) displays the dependency on the travel-distance.

In summary, Fig. (5.2) clearly demonstrates that within the realistic parameter ranges, a considerable amount of the attenuation can be explained in terms of scattering attenuation. Moreover, for frequencies higher than 30 Hz, all relevant parameter combinations yield a quality factor smaller than 100. In contrast to previous interpretations (see above), this indicates that scattering on upper-crustal heterogeneities plays at least a considerable role at the KTB-site. We do not see a contradiction to the fluid-filled crack systems hypothesis as a possible source of strong attenuation since there would be also strong scattering attenuation on these crack systems. Nevertheless, a strong intrinsic attenuation in this area is also still possible. Especially for frequencies smaller than 30 Hz, the measured Q-values can not be explained in terms of scattering attenuation.

This study intends to clarify the role of scattering attenuation when interpreting seismic attenuation measurements. We may speculate whether other regions of the continental crust also exhibit similar scattering attenuation estimates like the KTB-site. The evidence that well-log statistics are quite uniform throughout the continental crust (Holliger, 1996) and the reported low Q-values (Pujol et al., 1998 for a review) support this hypothesis. Together with the constraints on absorption from laboratory measurements, such knowledge may contribute in the stochastic characterization of seismic heterogeneities in the lithosphere.

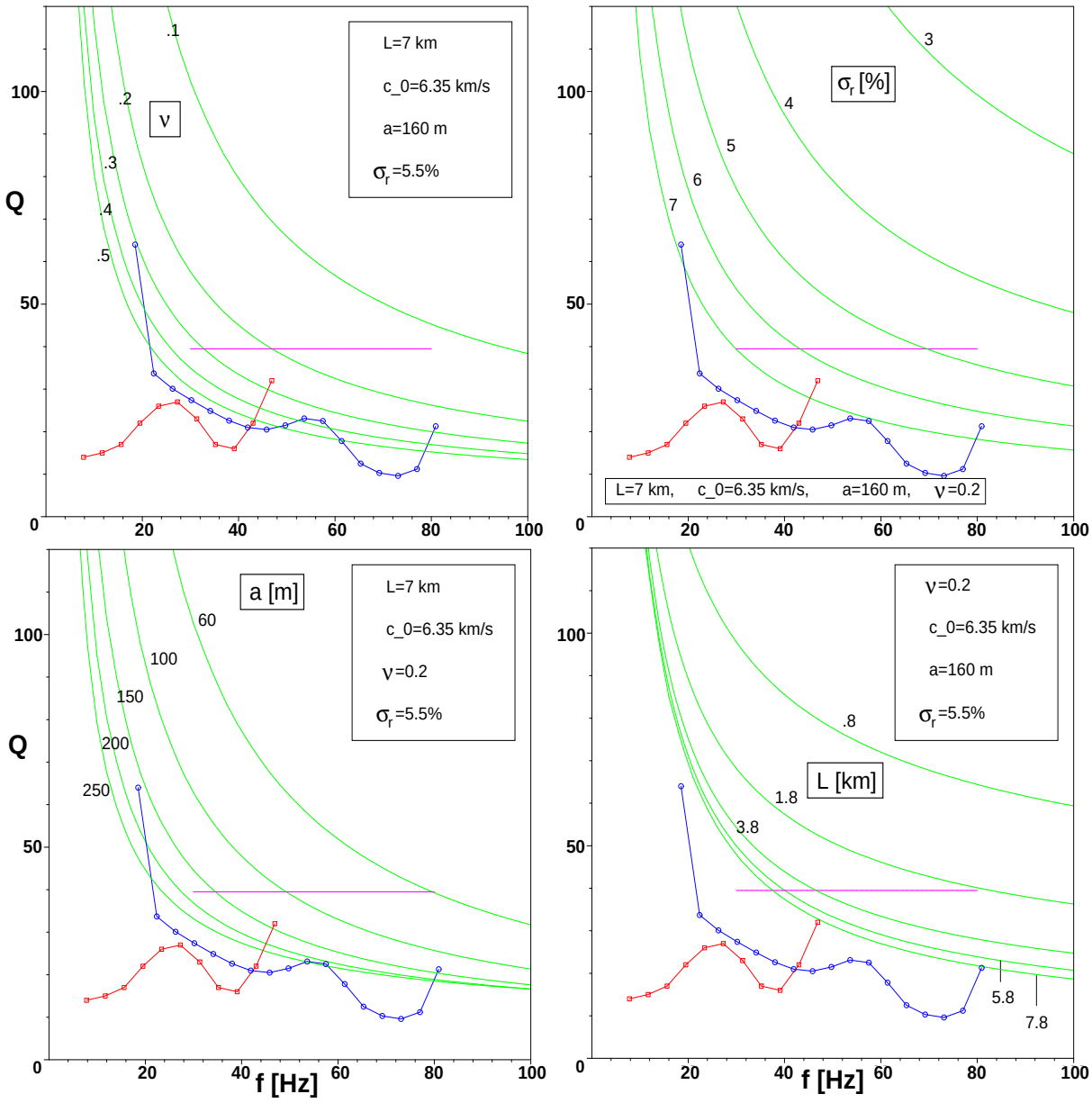

Figure 5.2: Parameter study of the scattering attenuation model using statistical estimates from well-log data at the KTB-site. The measured Q-values from Fig. (5.1) are displayed for comparison.

5.2 Correction for transmission losses

In chapter (3) we derived the Green's function for 2-D and 3-D random media

$$G(t,L) = \frac{1}{2\pi} \int_{-\infty}^{\infty} d\omega \, e^{iKL} e^{-i\omega t} \,, \tag{5.2}$$

describing the evolution of the primary wave field when the incident wave is a δ-pulse. In some special cases it is possible to obtain explicit results (see the Gaussian pulse approximation in section 3.7.2). Here we introduce another quantity that is useful for the description of seismic wave fields, namely the time-harmonic transmissivity (which is in fact identical to the time-harmonic plane wave used in section 3.2)

$$T(t,\omega,L) = e^{i(KL-\omega t)} \,. \tag{5.3}$$

Apart from a phase shift, the transmission losses may then be characterized by the real function

$$T_{\text{loss}}(\omega,L) = e^{-\alpha(\omega,L)L} \,. \tag{5.4}$$

Compensating of the primary amplitude decrease is then possible by computing its inverse

$$T_{\text{loss}}^{-1}(\omega,L) = e^{\alpha(\omega,L)L} \,. \tag{5.5}$$

Since the scattering attenuation coefficient α is always larger or equal than zero, T_{loss}^{-1} is larger or equal than unity. It depends also non-linearly on travel-distance and on the fluctuation spectrum of the heterogeneities. To apply formula (5.5) in the time domain requires a fixed frequency ω_0. Its choice should reflect the frequency content of recorded signals. Therefore, the frequency corresponding to the maximum of the amplitude spectrum of the recorded wave field is a reasonable choice.

That transmission losses are an important issue in imaging and inversion has been recognized by various authors. For instance, Levander and Gibson (1991) analyzed reflection responses with help of numerical experiments in 2-D random media. Henstock and Levander (2000) investigated the effects on reflection amplitudes caused by a heterogeneous overburden. How the image quality is influenced by scattering structures is shown in Martini et al. (2001). However, no adequate concepts for compensation due to scattering have been proposed. In the case of thinly layered overburdens, the problem can be looked upon as solved some years ago (Widmaier et al., 1996, and Wapenaar & Herrmann, 1996). In the following we give two examples of common techniques in exploration seismology, where the compensation for transmission losses is an essential step in the amplitude processing.

5.2.1 Migration in the presence of a heterogeneous overburden

In order to obtain subsurface images with reliable amplitude information, one usually applies the true amplitude prestack Kirchhoff migration technique. The amplitudes are true in the sense that a weighting function depending on the subsurface coordinate and the receiver

coordinate essentially accounts for the effect of geometrical spreading.

Heterogenieties between receiver and reflector can not be handled within this migration scheme. However, the above derived Green's function takes into account these effects, namely the amplitude decrease with travel-distance and the pulse broadening of the primary wave field. The idea is now to combine both concepts. Thus, the effects of small-scale heterogeneities can be removed by convolving the wave field with the inverse Green's function. A simpler, but more efficient way in terms of computing time, uses equation (5.5). Then the convolution degenerates to a multiplication. Hence, the modified Kirchhoff integral is

$$M(\mathbf{x}) = \int\limits_{\mathbf{x}_{rcv}} W(\mathbf{x}, \mathbf{x}_{rcv}) \quad T_{\text{loss}}^{-1} \; u(\mathbf{x}_{rcv}, t_{dif}) \,, \tag{5.6}$$

where u is the observed wave field and W denotes the weighting function. The summation extends over all receiver positions along the corresponding diffraction curves t_{dif}. The migration result $M(\mathbf{x})$ attaches to each subsurface point $\mathbf{x}$ a certain (true-) amplitude value (for details regarding the implementation see Buske et al., 2001).

We test this correction method by numerical simulations. To attach a seismologically relevant meaning to the simulations, we create a simplified model of the Nazca plate subducting beneath South America. This subducting zone is a subject of the collaborative research project SFB267. The model essentially consists of two half-spaces, where the upper part is superimposed by statistically isotropic heterogeneities. Of course, the statistical properties of these fluctuations are a priori not known. Generally, statistical estimates can be extracted from well-log data or – in our case of deep reflection profiling – from statistical wave field analysis (Wu and Flatté, 1990). The corresponding seismic profile was obtained within the ANCORP96 experiment in the central Andes. The geometry and material parameters are described in Fig. (5.3). 50 seismograms (z-component of the wave field) from the 251 seismograms of a shot gather are displayed in Fig. (5.4).

Performing the prestack Kirchhoff migration without correction for transmission losses (i.e., $T_{\text{loss}}^{-1} = 1$) and picking the amplitude values along the reflector image yields the black and dashed-red curves in Figure (5.5). The black curve shows to the amplitudes values of the corresponding homogeneous reference model (when there are no fluctuations in the overburden). The decrease of the amplitudes outside the offset interval $[68km, 72km]$ is because in this single shot experiment only a part of the reflector is illuminated. The dashed-red curve is obtained for the model with heterogeneous overburden. Two effects can be observed: the covered part of the reflector (offset $\approx 66km$) shows lower amplitude values (18% less than in the homogeneous overburden case) and is shifted to the left. Moreover, the decrease of the amplitudes outside the covered part around $66km$ offset is superimposed by random fluctuations. Applying the Kirchhoff migration using formula (5.6) and picking the amplitudes along the imaged reflector yields the red curve in Figure (5.5). These corrected amplitude values reach the same level as those of the homogeneous case, indicating that the effect of the small-scale heterogeneities has been successfully removed.

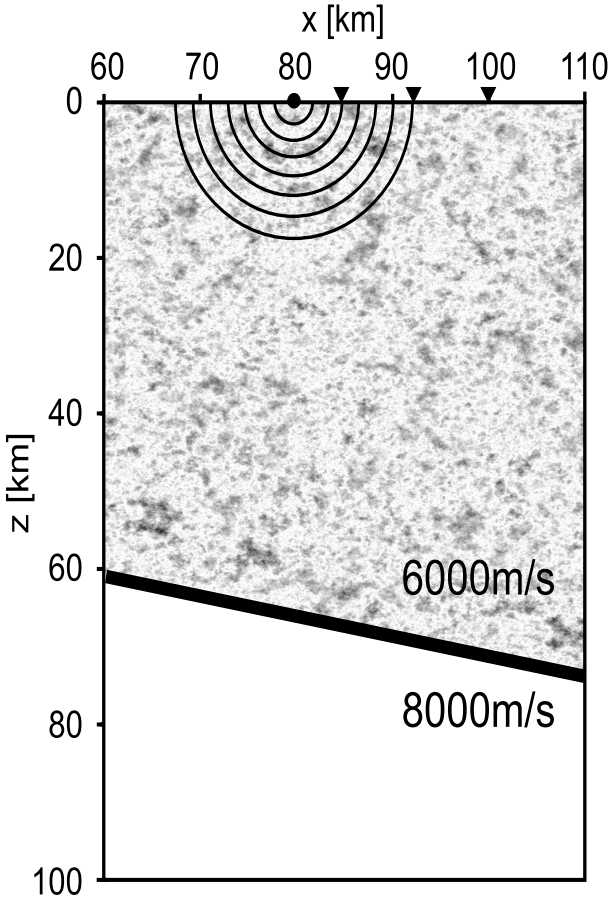

Figure 5.3: Simplified model of the subducting Nazca plate with a heterogeneous overburden. The overburden heterogeneities of the P-wave velocity are statistically characterized by an exponential correlation function with a standard deviation $\sigma = 1.5\%$ and a correlation length $a = 1km$. The background P-wave velocity in the upper part is $v_P = 6000m/s$ and below the reflector $v_P = 8000m/s$. The S-wave velocity and the density are derived from the P-wave velocity model using $v_S = v_P/\sqrt{3}$ and $\rho = (1.755 + 0.155v_P/1000)1000\,kg/m^3$, respectively. The ANCORP96 profile is simulated by placing a point-source (with a center-frequency of $15Hz$) at $x = 80km$ and recording the wave field at 200 geophones (equidistantly spaced) over an offset range of $20km$. Note that the whole velocity model is embedded into a constant velocity model such that no surface waves are generated.

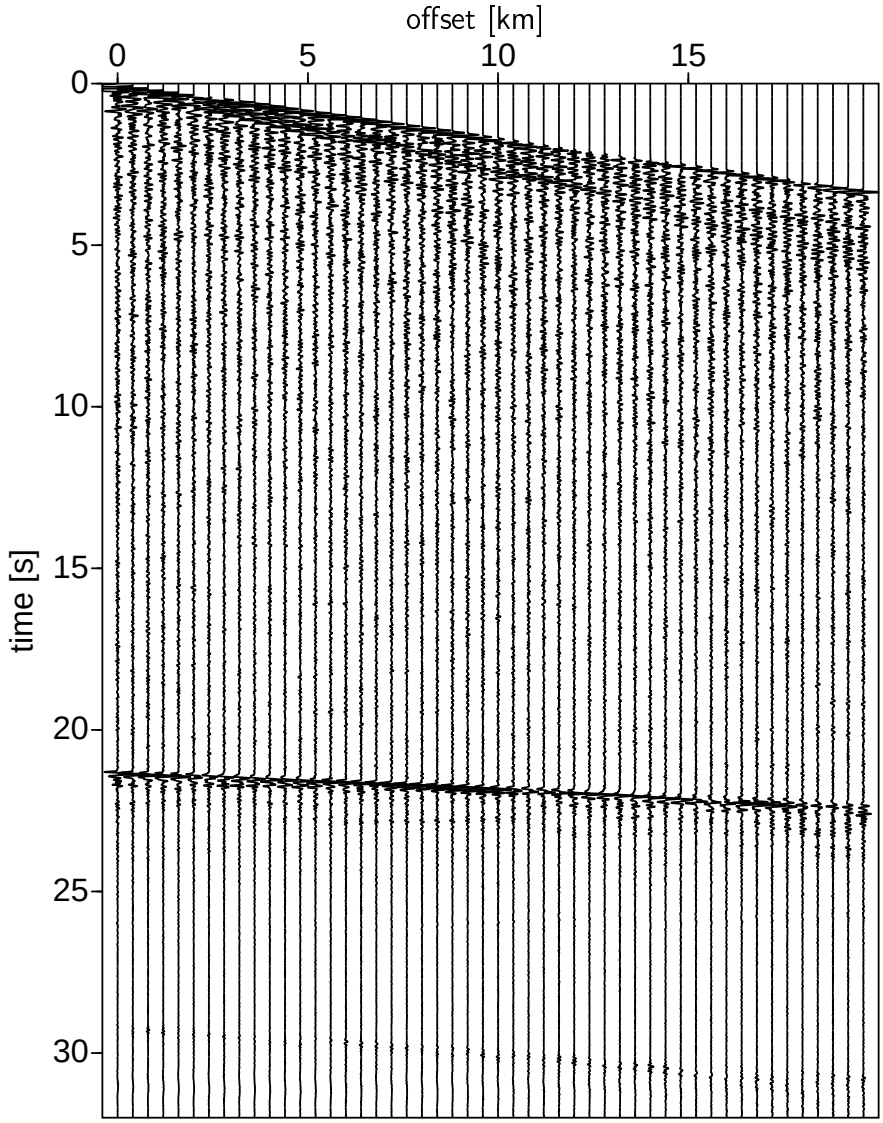

Figure 5.4: Seismograms of the shot gather. Note the increasing complexity of the waveforms with increasing offset. The events around $21s$ (two-way traveltime) correspond to the reflected P-wave.

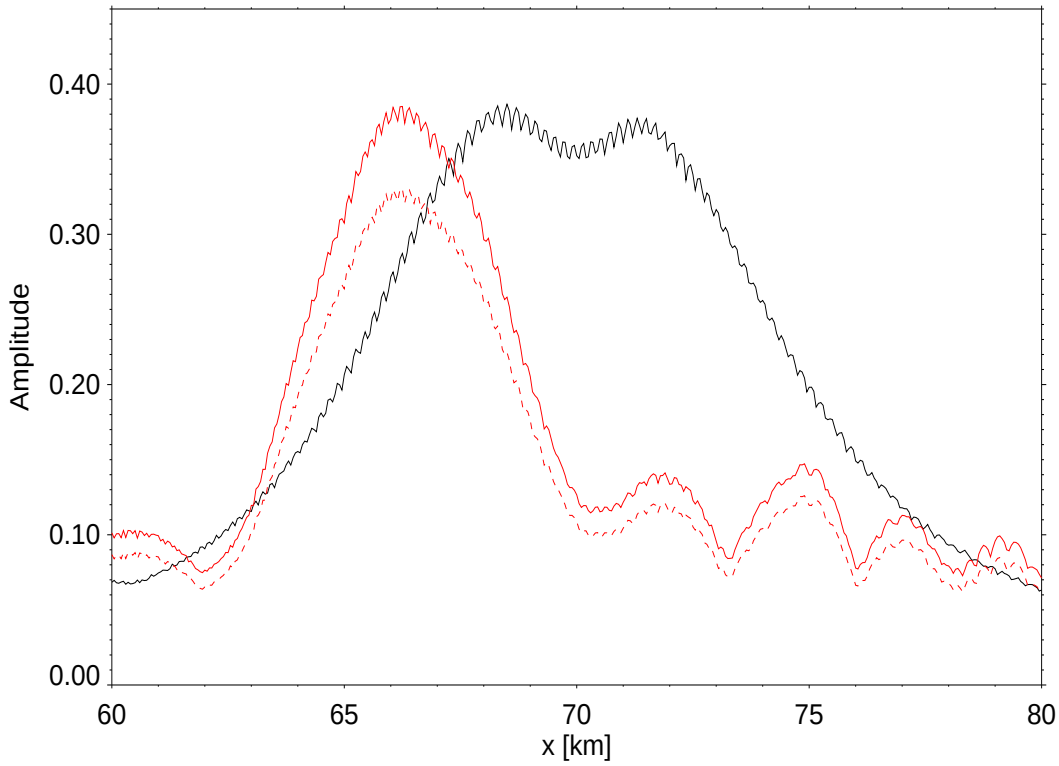

Figure 5.5: The picked amplitude values along the imaged reflector. The black and dashed-red curves correspond to the migration result from the homogeneous reference model and from the heterogeneous overburden model, respectively. The red curve shows the corrected amplitudes, i.e., the migration is based on formula (5.6) which accounts for transmission losses. Thus, the corrected (red) curve shows amplitude values that reach the same level of amplitudes than in the homogeneous reference model (black curve) indicating that the effect of the overburden heterogeneities has been successfully removed.

5.2.2 Improved AVO analysis

In hydrocarbon industry it is a common practice to perform so-called amplitude versus offset analysis (AVO). For a review we refer to Castagna (1993). To put it simple, amplitudes of identified waveforms (e.g. reflected P-wave) in common midpoint gathers are picked and corrected for geometrical spreading. The result is plotted versus the offset. These AVO curves can be fitted by curves that include assumptions of P- and S-wave velocity and density. This is possible because exact equations for angle dependent reflection/transmission coefficients are available in the form of the Zoeppritz equations. In that way a simple macro-velocity model can be constructed. The reflection coefficient can be computed by the ratio of reflected and incident amplitude. Reflection coefficients contain valuable information on lithology, porosity and pore fluid content.

In the following we are interested in the estimation of the reflection coefficient of a single seismic reflector. The situation is complicated by the fact that the space between recording position and reflector is not homogeneous. To take into account the effect of the small-scale heterogeneities (small with respect to the macro-model structure), we essentially apply the same correction method as in Widmaier et al. (1996), however, using the extended ODA theory.

So, the black curve in Fig. (5.7) corresponds to R_{PP} in the homogeneous reference model, i.e., where the fluctuations are zero. Then, one can apply the exact Zoeppritz equation or in the case of small offsets (small incidence angles) the approximation of Aki and Richards (1980). For zero offset $R_{PP} \approx 0.2$ and decreases slightly with offset. Within this small offset range, R_{PP} is practically a straight line. Now, analyzing the direct and reflected P-wave amplitudes of the seismic section (5.4) referring to the inhomogeneous model (5.3), leads to the blue dots in Fig. (5.7). Thus, the heterogeneous overburden is responsible for the R_{PP} fluctuations with offset. The transmission loss due to scattering becomes clearly visible: almost all inverted R_{PP} values are located below the the homogeneous reference model curve. Fitting the inverted R_{PP} values by a straight line (blue curve) yields that on average the R_{PP} estimates are 30% lower than that of the reflection coefficients in the absence of fluctuations. From this consideration one can conclude that transmission losses due to scattering may lead to serious misinterpretations of relection coefficients.

The recipe to compensate for these transmission losses is then the following: multiply each amplitude involved in the computation of R_{PP} with equation (5.5) using the corresponding travel-distance. This is an additional step in the usual amplitude processing and is indicated in Fig. (5.6). The result of this correction is shown in Fig. (5.7) by the red triangles. As expected, each R_{PP} value is now increased. To make the analysis more quantitative, these corrected R_{PP} are fitted by a straight line (red curve). Comparing the 'true' R_{PP} estimates represented by the black curve and the corrected R_{PP} estimates shows the performance of the correction method: In the investigated offset range the maximum error in estimating the reflection coefficient is less than 10%.

The above analysis may be criticized in some sense. The proposed correction method increases the fluctuations of R_{PP} and the straight line fit seems not to be justified. Moreover, implicitly we assume that R_{PP} does not vary along the reflector (compare with the previous

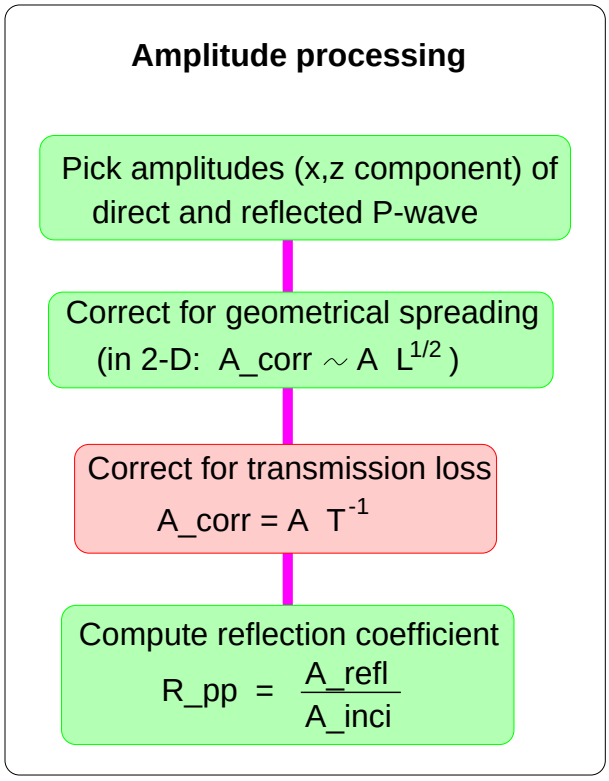

Figure 5.6: The applied amplitude processing including the correction for transmission losses as a new step.

section). The interaction between reflected P-wave and the scattered wave field are neglected. How these difficulties can be partially overcome is discussed in Sick et al. (2001). There it is shown that the fluctuations can be significantly reduced when using the data from more than one shot gather.

In summary, with help of a synthetic, idealized AVO study, we demonstrate the performance of the proposed correction method aiming at a compensation of transmission losses due to small-scale heterogeneities located in the reflector overburden. We think that this strategy can be used in practical situations in order to constrain and to increase the reliability in the estimation of reflection coefficients. Provided that statistical information of the random structure is available, the estimation of the reflection coefficient becomes more feasible.

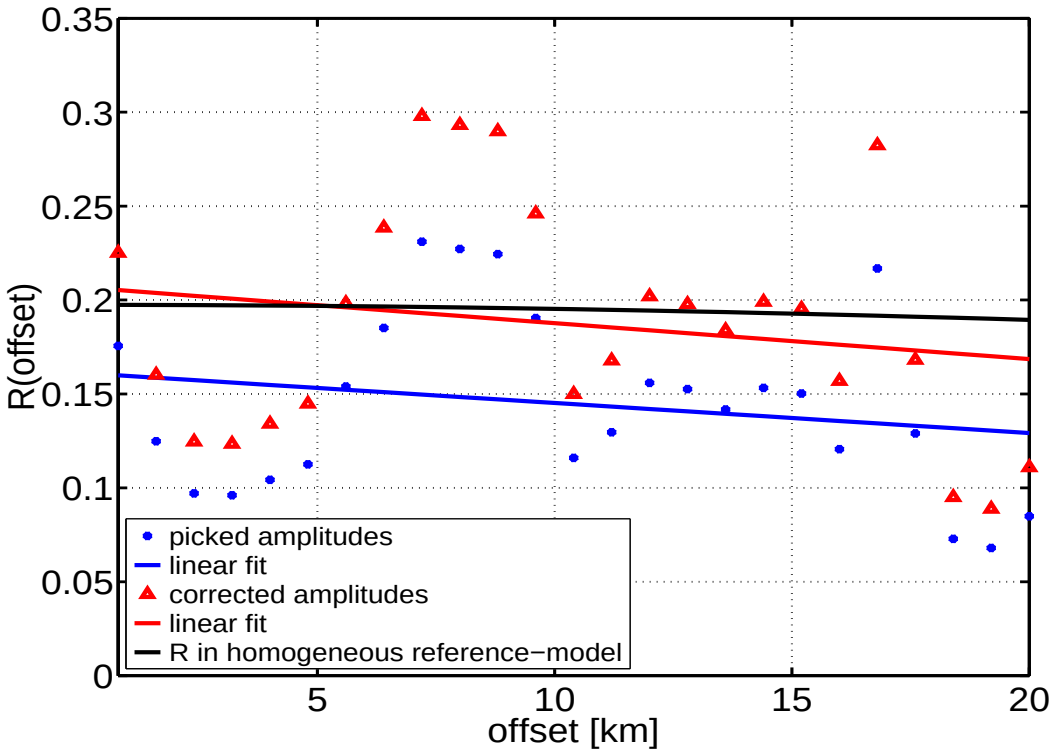

Figure 5.7: Reflection coefficient R_{PP} versus the offset. The black curve corresponds to the homogeneous reference model. R_{PP} estimates from the model with heterogeneous overburden is denoted by the blue dots (and the blue curve). After the correction the R_{PP} estimates are denoted by red triangles (and the red curve).